REPRODUCIBILITY OF RAPID SHORT ECHO TIME CSI AT 3T FOR CLINICAL APPLICATIONS

Sofie Van Cauter, MD [1], Diana M. Sima, PhD [2], Jan Luts, PhD [2] , Leon ter Beek, PhD [3], Annemie Ribbens, MSc [4], Ronald R. Peeters, PhD [1], Maria I. Osorio Garcia, PhD [2], Yuquan Li, MSc [2,5], Stefan Sunaert, MD PhD [1] , Stefaan W. Van Gool, MD PhD [6], Sabine Van Huffel, PhD [2] and Uwe Himmelreich, PhD [7]

Author affiliations:

1. Department of Radiology, University Hospitals Leuven, Leuven, Belgium

2. Department Electrical Engineering-ESAT/SCD, Catholic University Leuven, Leuven, Belgium

3. Philips Medical Systems, Best, The Netherlands

4. Department Electrical Engineering-ESAT/PSI, Catholic University Leuven, Leuven, Belgium

5. School of Electronical Engineering, University of Electronical Science and Technology of China, Chengdu, People's Republic of China

6. Pediatric Neuro-Oncology, University Hospitals of Leuven, Leuven, Belgium

7. Biomedical NMR Unit/Molecular Small Animal Imaging Center, Department of Imaging and Pathology, Catholic University Leuven, Leuven, Belgium

Corresponding author:

Sofie Van Cauter

Department of Radiology

Herestraat 49

3000 Leuven

Belgium – Europe

Tel: +32 16 34 90 69

Fax: +32 16 34 37 65

FOR PEER REVIEW ONLY

Abstract

Purpose: To validate the reproducibility of a chemical shift imaging (CSI) acquisition protocol with parallel imaging, using automated repositioning software.

Material and Methods: Ten volunteers were imaged three times on two different 3T MRI scanners, receiving anatomical imaging and two identical CSI measurements, using automated repositioning software for consistent repositioning of the CSI grid. Offcenter parameters of the CSI plane were analyzed. Coefficients of variation(CoV), Cramér-Rao lower bounds(CRLB), intraclass correlation coefficients(ICC) and coefficients of repeatability(CoR) for immediate repetition and between scanners were calculated for N-acetylaspartate, total choline, creatine, myo-inositol(Myo) and glutamine+glutamate. Proportions of variance reflecting the effect of voxel location, volunteer, repetition, time instance and scanner were calculated from an ANOVA analysis.

Results: The offcenter vector and angulations of the CSI grid differed less than 1 mm and 2° between all measurements. The mean CoV and CRLB were less than 30% for all metabolites, except for Myo. The variance due to voxel location in the volume of interest and the error represent the largest contributions in variability. The ICC is the lowest for Myo and Glx. CoR for immediate repetition and between scanners display values between 22 and 83%.

Conclusion: We propose a CSI protocol with acceptable reproducibility, applicable in clinical routine.

FOR PEER REVIEW ONLY

Key words: proton magnetic resonance spectroscopy; reproducibility; brain; healthy volunteer study; SENSE; chemical shift imaging

FOR PEER REVIEW ONLY

INTRODUCTION

Magnetic resonance spectroscopy (MRS) has already been used for decades to study the metabolic principles of diagnosis and staging of diseases, therapeutic response assessment and disease progression (1-3). However, MRS is still scarcely used in routine diagnosis when compared to MR imaging (MRI) techniques. This is due to time-consuming acquisition protocols and operator intensive data analysis and interpretation. The lack of robust repositioning methods for longitudinal follow-up studies hinders the clinical applicability of MRS. With the advent of semi-automatic data acquisition, data processing and quantification, the interest in clinical use of chemical shift imaging (CSI) has increased (4,5). Robust repositioning methods also became available and should reduce variability due to imperfect repositioning of the CSI grid in consecutive MR examinations.

Increasing acquisition speed has always been a topic of major interest in the field of MRI and MR spectroscopy. Parallel imaging techniques provide an alternative to substantially decrease acquisition times. In parallel imaging techniques, a reduced number of phase-encoding steps, thus a reduced number of samplings in k-space, gives rise to a reduced FOV. The consequent aliasing is unwrapped by exploiting information of the spatial sensitivity profile of each individual coil element in the phased array coil. The simultaneous acquisition of signals from different coil elements yields the scan time reduction (6). Different parallel imaging techniques have been developed, such as SMASH (simultaneous acquisition of spatial harmonics) (7), SENSE (sensitivity encoding) (8) and GRAPPA (generalized autocalibrating partially parallel acquisitions) (9). In this study, we apply SENSE in combination with 2D-CSI, reducing the acquisition time by decreasing the number of phase encoding steps in the two spatial dimensions with adequate reconstruction

FOR PEER REVIEW ONLY

based on the sensitivity profiles of the different coil element in the phase array-coil. As MR imaging in clinical setting often benefits from a multimodal imaging combining different advanced MRI techniques, a CSI protocol with a clinically acceptable acquisition time is of considerable interest to improve the implementation MR spectroscopy in routine clinical setting.

Definition of data quality, assessment of quality assurance, robustness of quantification methods and parameter optimization are of utmost importance to fully exploit the CSI technique. The literature concerning this topic is relatively limited in comparison to an increasing number of publications on clinical studies and experimental use of CSI. Reproducibility studies are an important aspect of data quality assessment and take into account the effects of acquisition and quantification. Testing the reproducibility of acquisition protocols and data processing methods is needed to objectively evaluate pathologic changes in patients and animals and to obtain the definition of normal ranges. A good reproducible method guarantees the most sensitive detection of pathology. When significant changes are observed from the established normal values, these results are likely to represent alterations due to pathology, rather than physiological metabolite variability, intrinsic errors from the technical equipment or inaccuracies in quantification (10).

The purpose of this study is to validate the reproducibility of a short echo time 2D-CSI acquisition protocol combined with the parallel imaging technique SENSE using the PRESS volume selection method in two different MR scanners in our institute repeatedly on the same healthy volunteers. Additionally, we want to investigate the potential additional value of automated repositioning software of anatomical sequences in the robustness of the manual placement of the CSI grid in longitudinal experiments.

FOR PEER REVIEW ONLY

MATERIAL AND METHODS

Study Setup

Ten healthy volunteers (age range: 23-35 years; average age: 28 years, 4 males/ 6 females) participated in this study (Fig. 1, top panel). Informed consent was obtained from all participants and the study was in agreement with the regulations and guidelines of the institutional review board. Every volunteer was imaged at six time instances in total, three times on two different 3 Tesla (T) MR scanners (Achieva Tx and Intera, Philips, Best, The Netherlands) in our institute, using the body coil for excitation and a receive-only eight-channel phased array head coil for signal reception. In every imaging session, the CSI measurement was immediately repeated without repositioning of the volunteer nor the CSI grid, in order to test variability intrinsic to the acquisition method. Variability between scanner platforms was tested by repeating scans for each volunteer at both platforms. In addition, variability due to positioning errors and potential metabolic variability was tested by scanning each volunteer on the same platform for a second and a third time point. In total, 120 CSI datasets were acquired. All scans were finished within two weeks.

Imaging Protocol

An axial spin echo T2-weighted image (TR/TE= 3000/80 ms, slice/gap: 4/1 mm, Turbo Factor (TF): 10, field of view (FOV): 230 mm x 184 mm, matrix: 400 x 300) was acquired as a high-resolution anatomical reference image. The T2-image was positioned on a 3D T1-weighted low resolution survey scan (sagittal acquisition,

FOR PEER REVIEW ONLY

TR/TE: 3.1/1.4 ms, TFE: 26, FOV: 250 mm (feet-head: FH) x 250mm (anterior-posterior: AP) x 220 mm (left-right: LR); matrix: 112 x 112), using automated repositioning software commercially provided by the vendor (SmartExam, Achieva 3.0 Tesla MR System, Release 2.1, Philips Healthcare, Best, The Netherlands). The technique of the automated scan prescription is described in detail elsewhere (11). Generating the plan geometry to position the high-resolution T2-weighted image had a processing time less than 10 seconds. In this automated scan planning process, the FOV of the high-resolution anatomical images is aligned along anatomical landmarks, e.g. the anterior/posterior commissure, the vertex or the protuberantia occipitalis, on the low-resolution survey scan. In our institute, anatomical landmarks were set to the anterior and posterior commissure and the mid-sagittal plane on the 3D survey scan. A reference scan was performed to obtain the sensitivity information of the multiple phase–array coils, used in the SENSE reconstruction (TR/TE: 4.0/0.79 ms, FOV: 450mm x 300mm, matrix: 96 x 50) . After acquiring the anatomical scans, the two-dimensional (2D) CSI matrix was manually positioned on the T2 images at two slices above the last slice in which the ventricles are visible, symmetrically around the midline with the anterior margin of the FOV coinciding with the frontal skull. (Fig.1, lower left panel) The 2D-CSI protocol had the following imaging parameters: the point-resolved spectroscopy (PRESS) was used as the volume selection technique (12) with a bandwidth of 1.3 kHz of the conventional slice selective pulses, TE: 35 msec, TR: 2000 msec, FOV: 16 cm x 16 cm, volume of interest (VOI): 8 cm x 8 cm, slice thickness: 1 cm, acquisition voxel size: 1cm x 1cm, reconstruction voxel size: 0.5 cm x 0.5 cm, receiver bandwidth: 2000Hz, samples: 2048, number of signal averages: 1, carrier frequency of the water suppressed file was set to 2.2 ppm, in the unsuppressed water spectrum the carrier frequency was

FOR PEER REVIEW ONLY

set to 4.7 ppm, water suppression method: MOIST (multiple optimizations insensitive suppression train), a vendor provided water suppression technique that implements a series of four very selective pulses designed for B1 and water T1 insensitivity, a modification of the WET technique (13), high order (first and second order) pencil beam shimming, parallel imaging technique SENSE with reduction factor R: left-right: 2, anterior-posterior: 1.8 (total reduction factor: 3.6), 10 circular 30-mm outer-volume saturation bands in order to avoid lipid contamination from the skull. Automated prescanning optimized the shim by using phase mapping, performed the water suppression and set both transmitter and receiver gains. The acquisition time was 3 minutes, 30 seconds.

Data Analysis

To validate the reproducibility of the positioning of the CSI grid, we analyzed the offcenter parameters of the CSI plane between the measurements at different time instances within each volunteer. The length of the three dimensional vector off the isocenter of the magnet is defined as

$$|(A,B,C)^T| = \sqrt{(A^2 + B^2 + C^2)} \qquad [1]$$

with *A* representing the range off center in the anterior-posterior direction, *B* representing the range off center in the left-right direction and *C* the range off center in the cranio-caudal direction. Furthermore, the angulations off the isocenter of the magnet in the anterior-posterior, left-right and cranio-caudal plane were considered. The slice of the T2-weighted image on which the CSI grid was positioned, was segmented in cerebrospinal fluid (CSF), grey and white matter, using in house software in order to test how much difference in partial volume between repeated measurements is responsible for the reported offset vector and angulation difference.

FOR PEER REVIEW ONLY

CSI data were checked upon quality as recommended in Kreis, 2004, i.e., we computed signal-to-noise ratios for all voxels in all grids using both time-domain and frequency-domain formulations, and linewidths of the unsuppressed water signals (10). The MR spectra were processed as follows using the MATLAB 2010b environment (MathWorks, Massachusetts, U.S.A.).

Taking into consideration a bandwidth of 1.3 kHz of the conventional slice selective pulses, the chemical shift displacement effect (CSDE) at 3T is +/- 35% over 3.5 ppm (water - fat shift). In that view, we truncated the three outer rows (the outer two rows from the top, the outer line from the bottom, two columns from the right and one column from the left) in the 16 x 16 grid of the VOI in order to remove the edges of the CSI grid in the phase encoding directions, mostly affected by the chemical shift displacement effect. The residual water peak was filtered by the black-box method HLSVD-PRO (Hankel-Lanczos singular value decomposition with partial reorthogonalization) (14) with passband 0.25-4.2 ppm and model order 30. Time domain signals were truncated to 512 points. Baseline correction was performed as part of the quantification step by a substraction procedure similar to (15): first, 4 points were truncated from the beginning of the FID. The truncated signals were preliminarily fitted with the metabolites of interest, as described below. A baseline estimate, obtained from smoothing the difference between the original signal and a back-extrapolated metabolite model, was consequently subtracted from the initial signal (512 points). No apodization was done prior to quantification. The AQSES-MRSI quantification method (16) was used for fitting the 9 most representative metabolites in the remaining 13*13 matrix: N-acetyl aspartate (NAA), glutamine (Gln), glutamate (Glu), creatine (Cre), phosphorylcholine (PCh), glycerophosphorylcholine (GPCh), myo-inositol (Myo), and macromolecules/lipids (Lip) at 0.9 and 1.3ppm,

FOR PEER REVIEW ONLY

referred to as Lip1 and Lip2 respectively. Glu + Gln and PCh + GPC are reported as Glx and tCho (total choline), respectively.

For comparison of metabolite values at the same location in different grids, the metabolite signal intensities in each voxel were normalized to the corresponding unsuppressed water signal in that voxel. Metabolite values in arbitrary (institutional) units are not further corrected for partial volumes or relaxation effects, thus no absolute concentrations are reported (17).

Signals of an in-house measured metabolite database were used for quantification. The metabolite basis set was composed of 16 metabolite solutions that were prepared as described before [1]: Cre, PCh, GPCh, lactate (Lac), Glu, gamma-aminobutyraat (GABA), carnitine (Car), NAA, glucose (Glc), aspartate (Asp), glycine (Gly), alanine (Ala), citrate (Cit), taurine (Tau) and Myo. Metabolite solutions were prepared according (18). The temperature was maintained at 37℃ and monitored using a temperature probe and the SAII software from Small Animal Imaging Inc (New York, USA). The pH was kept constant at 7.0 with a buffer solution.

Statistics

In each voxel of the VOI, the coefficient of variation (CoV) was computed for the concentration of representative metabolites (NAA, tCho, Cre, Glx and Myo) as the standard deviation divided by the mean of measurements of all 12 CSI acquisitionsfor each volunteer, as described before (19,20). These values show the observed variability in the estimated metabolites. Additionally, the metabolite quantification procedure AQSES-MRSI provides estimates of the Cramér-Rao lower bounds

[1] (http://s-provencher.com/pub/LCModel/manual/manual.pdf)

FOR PEER REVIEW ONLY

(CRLB) (21), which give an indication about the uncertainty of the estimated parameter values at a given noise level. Thus, if the CRLB is divided by the mean of measurements, it becomes directly comparable in size to the CoV. In theory, CRLB of any unbiased estimator should be smaller than the observed variability shown by CoV, but since AQSES-MRSI imposes constraints aimed at a more robust fitting, the estimation is no longer guaranteed to be unbiased and thus CoV may sometimes get smaller than the predicted CRLB.

In order to estimate the variance associated with the different measurement factors, an N-way-ANOVA analysis was performed with “scanner“ as fixed factor and with “volunteer”, “immediate repetition”, “time instance” and “location” (i.e. voxel position in the VOI) as random factor. Thus, for each metabolite separately, the mixed model was of the form

$$Y_{abcde} = \mu + V_{location,a} + V_{volunteer,b} + V_{repetition,c} + V_{time,d} + V_{scanner,e} + \varepsilon_{abcde} \qquad [2]$$

where Y_{abcde} is a variable representing the observed metabolite value which was estimated by AQSES; μ represents the overall mean of that metabolite over all voxels in all volunteers, repetitions, time instances and both scanners; $V_{location,a}$, $V_{volunteer,b}$, $V_{repetition,c}$, $V_{time,d}$ represent random variables with zero mean and variances $\sigma^2_{location}$, $\sigma^2_{volunteer}$, $\sigma^2_{repetition}$, σ^2_{time}, respectively, and account for the effect of “location” *a*, “volunteer” *b*, “immediate repetition” *c*, and “time instance” *d,* respectively. Additionally, $V_{scanner,e}$ stands for the fixed effect of the particular scanner, and ε_{abcde} represents the residual error term, also a random variable with zero mean and variance σ^2. The error term may be attributed to noise in the signals and the inherent

FOR PEER REVIEW ONLY

limitation of the quantification accuracy, but it should be understood more generally, as having a variance not accounted for by any other factor in the model.

The ANOVA analysis provides us with sum-of-squares (SS) values of the deviations from the overall mean for each factor separately, as well as for all factors in total. For the latter, all available measurements of one metabolite in all volunteers at all locations, i.e., all CSI grids and all their voxels, are used. On the other hand, to compute the SS for, e.g., the *location* factor, the estimated metabolite values for each metabolite are first averaged over all other factors (i.e., over all 10 volunteers and all available repetitions), and then the deviations from the overall mean are computed, squared and summed up over all the voxels in a grid. Similar computations are done for each of the other factors, by averaging out over the rest of the factors.

From these sum-of-squares, we computed η^2 values for each metabolite and each factor, i.e., the ratios between the sum of squares of deviations per factor from the overall mean (SS_{factor}) and the total sum of squares (SS) of deviations from the overall mean (SS_{total}),

$$\eta^2_{factor} = SS_{factor}/SS_{total}. \qquad [3]$$

This is a measure of effect size indicating the percentage of the total variability within the values of a metabolite, associated with the concerned factor.

Subsequently, we made use of the variances estimated by the ANOVA analysis. Recall that ANOVA provides estimates for the variances $\sigma^2_{location}$, $\sigma^2_{volunteer}$, $\sigma^2_{repetition}$, σ^2_{time}, and σ^2_{error} mentioned above, disentangling the observed variability in the estimated metabolites along the considered factors. From these estimates, we compute the intraclass correlation coefficients (ICC) between the first and second immediately

FOR PEER REVIEW ONLY

repeated measurements in all the data sets. These ICCs are computed as the ratio between the sum of estimated variances $\sigma^2_{location} + \sigma^2_{volunteer} + \sigma^2_{time}$ for the random factors other than "immediate repetition" and the total sum of variances $\sigma^2_{location} + \sigma^2_{volunteer} + \sigma^2_{repetition} + \sigma^2_{time} + \sigma^2_{error}$ .The scanner factor, considered fixed, does not have an associated estimated variance, thus it does not appear in the ICC computation. The ICC has a similar interpretation to a correlation coefficient, being closer to 1 as the agreement between the first and second immediate repetitions increases. The ICC captures in a single number the agreement between the immediate repetitions. Therefore, different metabolites can be directly compared.

In order to test for agreement between quantified metabolite values in immediate repetition (repeatability or test-retest reliability), coefficients of repeatability were produced. The coefficient of repeatability (CoR) is a measure of the 95% limits of agreement (LoA), as proposed originally by Bland and Altman (22), and is calculated in this study as 2 times the standard deviations of the differences $D_k = M_k^{repetition1} - M_k^{repetition2}$ between the repeated measurements of the same metabolite value, $M_k^{repetition1}$ and $M_k^{repetition2}$, assuming that the main difference is zero. By definition, this value provides the range of metabolite values in which 95% of test-retest measurement differences are situated. We report the CoRs as percentages of the mean metabolite amplitudes within each voxel for each considered metabolite. Specifically,

$$CoR = 2.\frac{\sqrt{\left(\frac{1}{n-1}\sum_{k=1}^{n}\left(D_k - \overline{D}\right)^2\right)}}{\overline{M}} \qquad [4]$$

FOR PEER REVIEW ONLY

where $\overline{M}$ is the mean value over all measurements of the same metabolite in the same location, *n* is the total number of acquisition sessions, and $\overline{D} = \frac{1}{n}\sum_{k=1}^{n} D_k$. (Note that Wijnen et al. and Wiedermann et al report almost the same formula as the CoR above (without the factor 2 (23,24)) under the name coefficient of variation (CoV)).

Furthermore, we tested for agreement between scanners. CoR between scanners were calculated with an adapted version of the coefficient of repeatability that takes into account the presence of repeated measurements for each volunteer . Specifically the differences $D_k = M_k^{scanner1} - M_k^{scanner\,2}$ are computed between averaged values of metabolite estimates among all (up to 6) measurements made on each scanner, for each volunteer at each location,, $M_k^{scanner1}$ and $M_k^{scanner\,2}$, assuming that the main difference is zero. To account for variance of the repeated measurements on each scanner, within-subject variance terms for both scanners are added in the numerator of the CoR formula above, following (Bland&Altman, 1999, formula (5.3))(25). In the results, CoRs between scanners are also presented as percentage of the mean metabolite amplitude, as explained above.

Furthermore, statistical analysis was performed on the segmented data in the T2-weighted images. In order to estimate the variance associated with the different measurement factors, an N-way-ANOVA analysis was performed with “scanner“ as fixed factor and with “volunteer”, “time instance” and “location” (i.e. voxel position in the slice T2-weighted images) as random factor. This was done in analogy with the statistical analysis of the metabolites. The factor “immediate repetition” was not included as we only acquired one high- resolution T2-weighted image in every time instance. From the ANOVA analysis, we computed η^2 values for each tissue type and

FOR PEER REVIEW ONLY

each factor. As there were no immediately repeated measurements for the anatomical data, ICC were not considered.

Statistical analysis was performed in Matlab, with the exception of the ICCs, which were computed from the variance estimates of ANOVA model fitting in SAS (SAS Institute Inc., Cary, USA).

RESULTS

Automated Repositioning Software

The automated scan planning was successful for the MR examinations in all 60 scan sessions in the ten volunteers. In the 60 scans, there was no difference in offcenter coordinates between the first and second CSI measurements. The offset vector of the CSI grid differed 0.55 +/- 0.13 mm (mean and standard deviation, respectively) between the 60 cases. The difference in angle between the reference line from the anterior to the posterior commissure adopted in the automated positioning of the high-resolution T2-image, and the transverse plane of the CSI grid, was less than 2° between all 60 cases (anterior-posterior angulation: 0°, left-right angulation: 0.02 +/- 0.06°, cranio-caudal angulation: -0.38 +/- 0.88°, mean and standard deviation, respectively).

Table 1 shows the variance attributed to a given factor for each tissue type in the slice of the T2 image on which the CSI grid was positioned. $\eta^2_{\text{time instance}}$ and η^2_{scanner} are almost negligible (reported as 0, absolute values in the range of 1e-5). The

FOR PEER REVIEW ONLY

variance due to the subjects is also very low (less than 0.5%). The voxel location accounts for the factor of the largest variability.

CSI Measurements

CSI data from one volunteer in one time instance (two datasets) had to be rejected due to significant sideband artifacts. The remaining 118 datasets were used for preprocessing and quantification. Signal-to-noise levels computed in the time domain (TD) and in the frequency domain (FD), according to the definitions in Kreis (10), ranged between 15 and 35 and from 8 to 18 respectively.

Spectral modeling of the water-unsuppressed measurements produced consistent full width at half maximum (FWHM) line width of the water peak of 16 +/- 3.8 Hz, slightly unevenly distributed in the CSI grid, i.e., lower values are found in the center (14 +/- 2.4 Hz) as opposed to the corners of the CSI grid (19 +/- 5.6 Hz) (Fig.1).

An example of the placement of the CSI grid and the selection of the definitive 13 x 13 matrix for quantification and analysis is shown in figure 2 (lower right panel). The quantified spectra and the residuals from the voxel indicated in figure 2 along the course of the experiment in one volunteer is shown in figure 3, indicating proper fitting of the metabolites and the baseline (minimization of the residual).

Overall Reproducibility And Variance

The CoV in the 13 x 13 central locations of the VOI in the 118 cases were (mean +/- standard deviation) 11 +/- 2% for NAA, 12 +/- 3% for Cre, 17 +/- 5% for tCho, 30 +/- 12% for Myo and 15 +/- 5% for Glx. (Fig. 4)

FOR PEER REVIEW ONLY

The CRLB in the 13 x 13 central locations of the VOI in the 118 cases were (mean +/- standard deviation) 14 +/- 2% for NAA, 18 +/- 6% for Cre, 29 +/- 13% for tCho, 55 +/- 38% for Myo and 11 +/- 3% for Glx. (Fig. 4). As described in the M&M section, the CSDE at 3T is +/- 35% over 3.5 ppm (water - fat shift) considering a bandwidth of 1.3 kHz of the slice selective pulses. In that perspective, we considered the CRLB of the metabolites in the central 9x9 grid, i.e. after removal of the two outer rows and columns on each side of the VOI (13 x 13), as we believe that this is the part of the VOI completely not affected by the CSDE. In this region, CRLB are 13 +/- 1% for NAA, 15 +/- 1% for Cre, 22 +/- 2% for tCho, 37 +/- 3% for Myo and 9 +/- 1% for Glx.

Analysis Of Variance Components

The ICC and η^2 values for each metabolite and each factor are reported in Table 2. Although η^2 values vary among metabolites some trends can be deduced. $\eta^2_{\text{immediate repetition}}$ and $\eta^2_{\text{time instance}}$ account for less than 0.16% of the overall variance in all metabolites whereas η^2_{scanner} represents less than 1.2% of the overall variance for all metabolites. $\eta^2_{\text{volunteer}}$ accounts for less than 5% of the variance. η^2_{location} (variance due to voxel position in the VOI) and the error account for the largest contributions in variability (over 50% for all metabolites and ranging from 17 till 49% respectively). The ICC is highest for NAA, tCho and Cre and clearly decreases for Glx and Myo.

Test-retest Reliability And Coefficients Of Repeatability Between Scanners

CoR for immediate repetition (test-retest reliability) averaged over the selected 13 x 13 grid in the 118 cases display mean values and standard deviations of 22 +/- 4%, 28 +/- 8%, 43 +/- 16%, 48 +/- 18% and 83 +/- 43% for NAA, Cre, tCho, Glx and Myo respectively for the 118 examinations. (Fig. 5, left panel) In the central 9x9 grid, CoR

FOR PEER REVIEW ONLY

for immediate repetition were 22 +/- 4%, 24 +/- 4%, 39 +/- 8%, 38 +/- 8% and 57 +/- 13% for NAA, Cre, tCho, Glx and Myo respectively for the 118 examinations.

CoR between scanners averaged over the selected 13 x 13 grid in the 118 cases display mean values and standard deviations of 25 +/- 3%, 28 +/- 8%, 41 +/- 14%, 35 +/- 12% and 73 +/- 31% for NAA, Cre, tCho, Glx and Myo respectively for the 118 examinations (Fig. 5, right panel). In the central 9x9 grid, CoR between scanners were 24 +/- 3%, 23 +/- 5%, 34 +/- 7%, 31 +/- 7% and 52 +/- 14% for NAA, Cre, tCho, Glx and Myo respectively for the 118 examinations.

DISCUSSION

One bottleneck preventing the more frequent application of CSI in clinical routine diagnosis is the time-consuming data acquisition. Three different approaches have been proposed to reduce acquisition time in CSI measurements: ellipsoid k-space encoding, parallel imaging reconstruction and echo planar spectroscopic imaging (26-29). Dydak et al. and Bonekamp et al. already demonstrated the feasibility of SENSE-CSI by proposing an acquisition protocol with a substantial reduction of scan time and preserved spectral and spatial resolution, still maintaining a reasonable SNR (26,30). However, their protocols still take more than 15 minutes. On the other hand, Bonekamp et al. were still able to perform good absolute quantification. As our main goal was to demonstrate a rapid CSI acquisition protocol, we did not aim at absolute quantification in return for decreased acquisition time. As SENSE is a parallel imaging technique operating in the image domain in which the sample size in the phase direction is decreased and the consequent aliasing is unwrapped by

FOR PEER REVIEW ONLY

exploiting information of the spatial sensitivity profile of each individual coil element in the phased array coil (31), the use of a 32-channel head coil could potentially yield better results with increased SNR, compared to the 8-channel head coil in our study. Although available in our institute, we decided to use the 8-channel head coil as our aim was to present a clinically feasible acquisition protocol and currently, the 32-channel head coil is not yet widely available. Using an 8-channel head coil with a geometry factor of 1.08 (32) and taking into account a reduction factor of 3.6 implies a loss in SNR of approximately 50%. However, the decrease in scan time is more than twofold, compared to no reduction factor. SNRs in our study were sufficient to result in reproducible quantification of the metaboliteswith the highest concentrations in the brain. Of interest to mention is that when the reduction factor used does not match the number of coil elements in the phase array coil, spatial aliasing causes spectral contamination (31). With emphasis on clinical cases, as stated by Zierhut et al. (29), aliasing of subcutaneous lipid contamination yields lipid signals in spectra which can possibly be mistaken for signs of necrosis of tumor. No evidence for aliasing was found in our data sets.

Longitudinal MR studies in patients with brain pathology are frequently performed to assess progression and therapy of diseases. Consistent scan planning with prospective or automated scan positioning has already been proven to yield reproducible inter- and intrasubject data with a greater accuracy than manual scan planning, even in the human brain with severely distorted morphology (11,33-35). Several techniques for prospective automated scan planning have been proposed. Van der Kouwe et al. presented an online method in which the brain is globally aligned to a statistical human brain atlas. Although their results are firm, this method is currently not applicable to the pathological human brain or other body parts than

FOR PEER REVIEW ONLY

the brain (35). Gedat et al. calculated offline the transformation matrix based on the geometrical coordinates to adapt the gradient reference frame in the follow-up examinations. They showed good results though the offline computation time proved to be the disadvantage of this method (36). Itti et al. segmented the brain surface on a fast 3D pilot scan, matched it offline with a high resolution surface scan of a test set and the alignment parameters were used to automatically plan subsequent scans according to desired geometry (37). Again, this technique has the disadvantage of potentially lower performance in severely distorted pathological brain. The method used in this study combines image recognition techniques to automatically identify landmarks in the human anatomy with afterwards a rough and a refined image registration to a mean model of the brain. Our results are in concordance with Gedat et al. reporting reported the most robust results of the above mentioned studies with a mean error of translational and rotational registration of 0.1mm and 0.2° respectively (36). The intra-subject variance and the inter-scanner variance in our anatomical data were almost negligible. Even the intersubject variance turned out to be very low. This additionally underscores the robustness of the repositioning software. Nelles et al. applied the automated scan planning technique used in this study in patients with severely distorted brain morphology and reported successful results of automated scan planning with only minor operator interactions required (11). Additional to the robust repositioning results, automated scan prescription accelerates, facilitates and elevates the quality of the workflow in clinical and experimental setting. In this study, the automated repositioning software of anatomical sequences was adopted to assess the robustness of the manual positioning of the CSI grid in an MR spectroscopy examination. Hancu et al. and Ratai et al. present a method of fully automated repositioning of single voxel and CSI

FOR PEER REVIEW ONLY

volumes respectively in subsequent examinations in patients (33,34). Although this technique proved to be robust, retrieving previous examinations of a particular patient is not always implementable, in particular when follow-up exams are scheduled with substantial time intervals.

^{1}H spectroscopy at high field strengths implies an increase in SNR, spectral resolution and ultimately increased quantification precision. However, the large spectral bandwidth at high field strengths also results in a substantial chemical shift displacement error of the slice selective refocusing pulses. This was apparent in our study when comparing equivalent voxels in both hemispheres (Fig.6). The use of adiabatic selective refocusing pulses with sharp selection profiles in combination with a conventional slice selective excitation while still maintaining echo times up to 30 ms as proposed by Scheenen et al. and Wijnen et al. in the semi-LASER sequence (23,38), is one possible solution to overcome those chemical shift displacement effects. Alternatively, a posteriori correction for the chemical shift displacement effect is possible by taking into account a voxel-wise calculated estimated fraction of the maximal PRESS excitation, though this approach is laborious and is difficult to implement in clinical routine (39). Tkac et al. clearly demonstrated the advantages of going to ultrahigh field strengths (4T and 7T) in clinical setting for single voxel MRS measurements reporting increased sensitivity and spectral resolution and consequently increased precision of metabolite quantification, when sufficiently dealing with B0 inhomogeneity by means of higher order shimming methods (40). Relating to our study, the variance due to voxel position in the VOI (i.e. factor “location”) proved to be the largest factor in the variability analysis. We believe that this is mainly due to the B0 inhomogeneity. Moreover, we assume that the difference of the full width at half maximum (FWHM) of the water peak between the center and

FOR PEER REVIEW ONLY

the outer borders of the VOI is caused mainly by the B0 inhomogeneity and to a lesser extent to the variability of the receiver coil profiles (41).

Several groups previously assessed variance and reproducibility of various CSI protocols on 3T as well as 1.5T, comprising 2D and 3D protocols of various durations with different echo times. Our goal was to present a clinically feasible CSI acquisition protocol, readily implementable in multimodal routine MR brain imaging. When comparing with other studies that have assessed the reproducibility of a CSI protocol at 3T, the CoV and CRLB obtained in this study are slightly higher than Maudsley et al. (41). Our reported CRLB are comparable to Ratai et al. (34). Due to a relatively low SNR, when compared to non-accelerated standard CSI protocols, we found slightly higher CRLB; which is also reflected in the analysis of variance in which the error factor accounts for the largest contributions in variability, apart from voxel location. The somewhat higher CoVs are possibly due to the fact that we did not perform segmentation for CSF and did not take into account the partial volume of grey and white matter in the CSI voxel, as it was not the purpose to represent absolute concentrations. Bonekamp et al. have applied SENSE-CSI for absolute quantification in a protocol with long TE and duration of 15 minutes and yielded robust results using an adapted phantom replacement technique (30). Furthermore, we did not take the partial volume effect into account to determine real inter-person and intra-person variability of metabolite levels. This has been done recently by another group. Gasparovic et al. demonstrated substantial improvements in both reproducibility and reliability of several metabolites with partial volume correction. The effect of partial volume correction on improving reproducibility is also evident on the ICCs. They consistently found higher ICCs for the data after partial volume correction (42).

FOR PEER REVIEW ONLY

We reported overall good reproducibility for the main metabolites NAA, Cho and Cre and Glx. Myo-inositol still imposed problems at the outer borders of the selected VOI and therefore changes in Myo should be carefully interpreted. Myo is inherently difficult to quantify as it is a metabolite with low concentrations having resonances in a region of the MR spectrum that heavily overlap with other metabolite resonances. Parts of the Myo signals (triplet at 4.05 ppm) can be distorted by imperfect water suppression (43). Less reproducible metabolites require greater changes compared to the established normal values before the observed alterations in metabolite concentrations can be assigned to true pathology rather than to inherent limitations of quantification and noise. For example, when implementing the proposed protocol, changes in Myo should be more than twofold in order to assign them to changes related to the studied condition.

Although our proposed rapid CSI acquisition protocol is not optimal to obtain absolute metabolite concentrations, the evaluated protocol (SENSE-CSI) may be useful for pattern recognition techniques or relative concentrations calculations for addressing clinical routine questions. In hospital settings, patient comfort and economical issues necessitate MR scan sessions with a limited time range. This conflicts with the upcoming trend in neuroradiology to evolve to a multimodal approach in order to asses complementary anatomical and physiological properties of the diseased brain. Therefore, we believe our proposed rapid acquisition protocol could be of interest to

FOR PEER REVIEW ONLY

implement in a combination with other functional MR imaging techniques like MR diffusion and perfusion imaging, for example, in the diagnosis of brain lesions, the grading of gliomas or the response assessment of brain tumors after therapy. An interesting result of this study was the small part of the variability attributed to the scanner. Furthermore, we demonstrated that the CoR between scanners were similar to the CoR for immediate repetition. This implies the possibility of interchanging the scanners in the follow-up patient examinations, an advantage in clinical setting.

In our proposed acquisition protocol, we applied the PRESS volume localization method with conventional slice selective pulses. As we did not use adiabatic slice selective pulses, the chemical shift displacement error of the slice selective refocusing pulses is substantial. The extent of the chemical shift displacement error does not influence the results of the reproducibility, though. However, the fact of having to exclude the outer edges of the VOI to retain interpretable spectra of sufficient quality is a considerable drawback when applying the proposed acquisition protocol.

In conclusion, we have conducted a reproducibility study to validate a rapid, short echo time 2D CSI acquisition protocol using the PRESS volume selection method. Rapid acquisition of CSI using SENSE (3:30 minute acquisition time for our protocol) may contribute in more widespread applications of MR spectroscopy for routine diagnostic applications. The robustness of vendor provided automated repositioning software for anatomical acquisitions was tested. Automated repositioning for anatomical sequences proved to be a very robust method, which is of utmost importance in conducting longitudinal studies. Comparison of MRSI data acquisition

FOR PEER REVIEW ONLY

on the same volunteers using different MR scanner indicates acceptable reproducibility, a pre-requisite for inter-institutional studies. However, great care should be taken for the interpretation of the results of metabolite signals with an inherent low SNR (e.g. Myo) as the error estimates are still substantial. Implementation of methods accounting for chemical shift displacement are essential for further improving rapid CSI techniques.

FOR PEER REVIEW ONLY

References

1. Graham GD, Barker PB, Brooks WM, et al. MR spectroscopy study of dichloroacetate treatment after ischemic stroke. Neurology 2000;55(9):1376-1378.
2. Gillard JH, Barker PB, van Zijl PC, Bryan RN, Oppenheimer SM. Proton MR spectroscopy in acute middle cerebral artery stroke. AJNR Am J Neuroradiol 1996;17(5):873-886.
3. Mathews VP, Barker PB, Blackband SJ, Chatham JC, Bryan RN. Cerebral metabolites in patients with acute and subacute strokes: concentrations determined by quantitative proton MR spectroscopy. AJR Am J Roentgenol 1995;165(3):633-638.
4. Morita N, Harada M, Otsuka H, Melhem ER, Nishitani H. Clinical Application of MR Spectroscopy and Imaging of Brain Tumor. Magn Reson Med Sci 2010;9(4):167-175.
5. Soares DP, Law M. Magnetic resonance spectroscopy of the brain: review of metabolites and clinical applications. Clin Radiol 2009;64(1):12-21.
6. Barker PB, Bonekamp D, Riedy G, Smith M. Quantitation of NAA in the brain by magnetic resonance spectroscopy. Adv Exp Med Biol 2006;576:183-197; discussion 361-183.
7. Lin DD, Crawford TO, Barker PB. Proton MR spectroscopy in the diagnostic evaluation of suspected mitochondrial disease. AJNR Am J Neuroradiol 2003;24(1):33-41.
8. Gass A, Davie CA, Barker GJ, McDonald WI, Miller DH. [Demonstration of plaque development in multiple sclerosis using magnetisation transfer ratio

FOR PEER REVIEW ONLY

images and protein spectroscopy with short echo time]. Nervenarzt 1997;68(12):996-1001.

9. Barker PB, Blackband SJ, Chatham JC, et al. Quantitative proton spectroscopy and histology of a canine brain tumor model. Magn Reson Med 1993;30(4):458-464.
10. Kreis R. Issues of spectral quality in clinical 1H-magnetic resonance spectroscopy and a gallery of artifacts. NMR Biomed 2004;17(6):361-381.
11. Nelles M, Gieseke J, Urbach H, et al. Pre- and postoperative MR brain imaging with automatic planning and scanning software in tumor patients: an intraindividual comparative study at 3 Tesla. J Magn Reson Imaging 2009;30(3):672-677.
12. Bottomley PA. Spatial localization in NMR spectroscopy in vivo. Ann N Y Acad Sci 1987;508:333-348.
13. Ogg RJ, Kingsley PB, Taylor JS. WET, a T1- and B1-insensitive water-suppression method for in vivo localized 1H NMR spectroscopy. J Magn Reson B 1994;104(1):1-10.
14. Laudadio T, Mastronardi N, Vanhamme L, Van Hecke P, Van Huffel S. Improved Lanczos algorithms for blackbox MRS data quantitation. J Magn Reson 2002;157(2):292-297.
15. Monsein LH, Mathews VP, Barker PB, et al. Irreversible regional cerebral ischemia: serial MR imaging and proton MR spectroscopy in a nonhuman primate model. AJNR Am J Neuroradiol 1993;14(4):963-970.
16. Croitor Sava AR, Sima, D. M., Poullet, J.-B., Wright, A. J., Heerschap, A. and Van Huffel, S. Exploiting spatial information to estimate metabolite levels in two-dimensional MRSI of heterogeneous brain lesions. NMR Biomed 2011;24.

FOR PEER REVIEW ONLY

17. Michaelis T, Merboldt KD, Bruhn H, Hanicke W, Frahm J. Absolute concentrations of metabolites in the adult human brain in vivo: quantification of localized proton MR spectra. Radiology 1993;187(1):219-227.

18. De Graaf RA. In vivo NMR spectroscopy: principles and techniques/ 2nd edition. Chicester, England: John Wiley and Sons, ltd: 2007.

19. Tedeschi G, Bertolino A, Campbell G, et al. Reproducibility of proton MR spectroscopic imaging findings. AJNR Am J Neuroradiol 1996;17(10):1871-1879.

20. Wu WE, Kirov, II, Zhang K, et al. Cross-sectional and longitudinal reproducibility of rhesus macaque brain metabolites: A proton MR spectroscopy study at 3 T. Magn Reson Med 2011;65(6):1522-1531.

21. Cavassila S, Deval S, Huegen C, van Ormondt D, Graveron-Demilly D. Cramer-Rao bounds: an evaluation tool for quantitation. NMR Biomed 2001;14(4):278-283.

22. Bland JM, Altman DG. Statistical methods for assessing agreement between two methods of clinical measurement. Lancet 1986;1(8476):307-310.

23. Wijnen JP, van Asten JJ, Klomp DW, et al. Short echo time 1H MRSI of the human brain at 3T with adiabatic slice-selective refocusing pulses; reproducibility and variance in a dual center setting. J Magn Reson Imaging 2010;31(1):61-70.

24. Wiedermann D, Schuff N, Matson GB, et al. Short echo time multislice proton magnetic resonance spectroscopic imaging in human brain: metabolite distributions and reliability. Magn Reson Imaging 2001;19(8):1073-1080.

25. Bland JM, Altman DG. Measuring agreement in method comparison studies. Stat Methods Med Res 1999;8(2):135-160.

FOR PEER REVIEW ONLY

26. Dydak U, Weiger M, Pruessmann KP, Meier D, Boesiger P. Sensitivity-encoded spectroscopic imaging. Magn Reson Med 2001;46(4):713-722.

27. Gu M, Liu C, Spielman DM. Parallel spectroscopic imaging reconstruction with arbitrary trajectories using k-space sparse matrices. Magn Reson Med 2009;61(2):267-272.

28. Posse S, DeCarli C, Le Bihan D. Three-dimensional echo-planar MR spectroscopic imaging at short echo times in the human brain. Radiology 1994;192(3):733-738.

29. Zierhut ML, Ozturk-Isik E, Chen AP, Park I, Vigneron DB, Nelson SJ. (1)H spectroscopic imaging of human brain at 3 Tesla: comparison of fast three-dimensional magnetic resonance spectroscopic imaging techniques. J Magn Reson Imaging 2009;30(3):473-480.

30. Bonekamp D, Smith MA, Zhu H, Barker PB. Quantitative SENSE-MRSI of the human brain. Magn Reson Imaging 2010;28(3):305-313.

31. Pruessmann KP, Weiger M, Scheidegger MB, Boesiger P. SENSE: sensitivity encoding for fast MRI. Magn Reson Med 1999;42(5):952-962.

32. Gizewski ER, Timmann D, Forsting M. Specific cerebellar activation during Braille reading in blind subjects. Hum Brain Mapp 2004;22(3):229-235.

33. Hancu I, Blezek DJ, Dumoulin MC. Automatic repositioning of single voxels in longitudinal 1H MRS studies. NMR Biomed 2005;18(6):352-361.

34. Ratai EM, Hancu I, Blezek DJ, Turk KW, Halpern E, Gonzalez RG. Automatic repositioning of MRSI voxels in longitudinal studies: impact on reproducibility of metabolite concentration measurements. J Magn Reson Imaging 2008;27(5):1188-1193.

FOR PEER REVIEW ONLY

35. van der Kouwe AJ, Benner T, Fischl B, et al. On-line automatic slice positioning for brain MR imaging. Neuroimage 2005;27(1):222-230.

36. Gedat E, Braun J, Sack I, Bernarding J. Prospective registration of human head magnetic resonance images for reproducible slice positioning using localizer images. J Magn Reson Imaging 2004;20(4):581-587.

37. Itti L, Chang L, Ernst T. Automatic scan prescription for brain MRI. Magn Reson Med 2001;45(3):486-494.

38. Scheenen TW, Klomp DW, Wijnen JP, Heerschap A. Short echo time 1H-MRSI of the human brain at 3T with minimal chemical shift displacement errors using adiabatic refocusing pulses. Magn Reson Med 2008;59(1):1-6.

39. Docchio F, Boulton M, Cubeddu R, Ramponi R, Barker PD. Age-related changes in the fluorescence of melanin and lipofuscin granules of the retinal pigment epithelium: a time-resolved fluorescence spectroscopy study. Photochem Photobiol 1991;54(2):247-253.

40. Tkac I, Oz G, Adriany G, Ugurbil K, Gruetter R. In vivo 1H NMR spectroscopy of the human brain at high magnetic fields: metabolite quantification at 4T vs. 7T. Magn Reson Med 2009;62(4):868-879.

41. Maudsley AA, Domenig C, Sheriff S. Reproducibility of serial whole-brain MR spectroscopic imaging. NMR Biomed 2010;23(3):251-256.

42. Gasparovic C, Bedrick EJ, Mayer AR, et al. Test-retest reliability and reproducibility of short-echo-time spectroscopic imaging of human brain at 3T. Magn Reson Med 2011;66(2):324-332.

43. Govindaraju V, Young K, Maudsley AA. Proton NMR chemical shifts and coupling constants for brain metabolites. NMR Biomed 2000;13(3):129-153.

FOR PEER REVIEW ONLY

Table 1

Analysis of variance components for the tissue types

	η^2				
	Time instance	**Volunteer**	**Scanner**	**Location**	**Error**
GM	**0**	**0.15**	**0**	**81.21**	**18.64**
WM	**0**	**0.46**	**0**	**86.48**	**13.06**
CSF	**0**	**0.43**	**0**	**54.75**	**44.82**

η^2 = proportions of variance; GM = grey matter; WM = white matter; CSF = cerebrospinal fluid

FOR PEER REVIEW ONLY

Table 2.

Analysis of variance components for the metabolites

	ICC	η^2 (%)					
		Immediate repetition	Time instance	volunteer	scanner	location	error
NAA	0.81	0.01	0.16	0.97	1.22	79.06	18.60
tCho	0.75	0.09	0.10	4.44	0	70.45	24.93
Cre	0.83	0.02	0.06	1.11	0.46	81.25	17.10
Glx	0.51	0.13	0.02	2.26	0.04	49	48.56
Myo	0.55	0.03	0.05	2.06	0.46	52.62	44.79

ICC = intraclass correlation coefficient; η^2 = proportions of variance; NAA = N-acetyl aspartate; tCho = total choline; Cre = creatine; Glx = total of glutamine and glutamate; Myo = myo-inositol

FOR PEER REVIEW ONLY

Figure Legends

Figure 1. Maps representing the mean water line width (left panel) and the standard deviation of the water line width (right panel).Remark a slight unevenly distributed FWHM line width of the water in the CSI grid with lower values are found in the center as opposed to the corners of the CSI grid.

Figure 2. An illustrative overview of the setup of the study is provided in the upper panel. The concept of the automated planning software adopted in this study is illustrated in the lower left panel. The position and geometry of the VOI are illustrated in the lower right panel. The selection of the 13 x 13 matrix for quantification is indicated by the red dots. The voxel of which the spectra are displayed in figure 2 is shown in yellow.**Figure 3.** Comparison of spectra from the 12 examinations in one healthy volunteer, obtained from the voxel indicated in yellow in figure 1. Left: Original spectra and their fits with AQSES-MRSI. Center: Difference between original spectra of repetition 1 and repetition 2 at each time instance; some frequency misalignments are noticeable. Right: Superimposed fits of the two repetitions, including frequency shift corrections.**Figure 4.** Maps of coefficient of variation (CoV) (left panel) and Cramér-Rao Lower Bounds (CRLB) (right panel) in the 13 x 13 matrix for NAA = N-acetyl aspartate; tCho = total choline; Cre = creatine; Glx = total of glutamine and glutamate; Myo = myo-inositol. Values are expressed in percentages.

Figure 5. Maps of coefficient of repeatibility (CoR) for immediate repetition (left panel) and between scanners (right panel) in the 13 x 13 matrix for NAA = N-acetyl aspartate; tCho = total choline; Cre = creatine; Glx = total sum of glutamine and glutamate; Myo = myo-inositol. Values are expressed in percentages.

FOR PEER REVIEW ONLY

Figure 6. Illustration of the chemical shift displacement error of the slice selective refocusing pulses. Three voxels compared between the left and the right hemisphere, selected from the VOI overlaid on the T2-weighted anatomical image. Note the asymmetrical intensities of the spectra from the left hemisphere (affected by the chemical shift displacement artefact) compared to the spectra from the right hemisphere (not affected by the chemical shift displacement artefact). Some lipid contamination due to insufficient outer volume suppression of subcutaneous lipisds is visible in the spectra from the right hemisphere. The red dots indicate the selection of the 13 x 13 matrix, used for quantification.

FOR PEER REVIEW ONLY

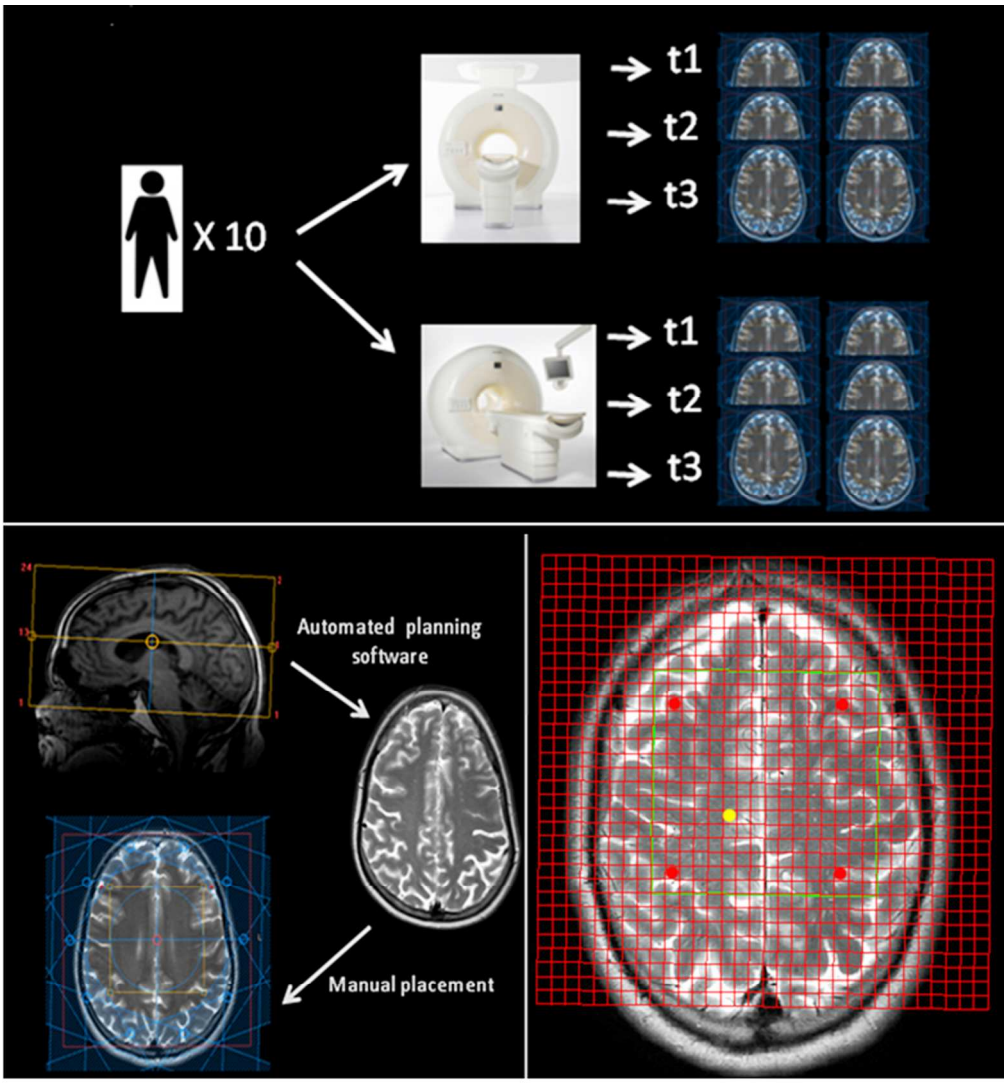


Figure 1. Maps representing the mean water line width (left panel) and the standard deviation of the water line width (right panel).Remark a slight unevenly distributed FWHM line width of the water in the CSI grid with lower values are found in the center as opposed to the corners of the CSI grid.
184x198mm (300 x 300 DPI)

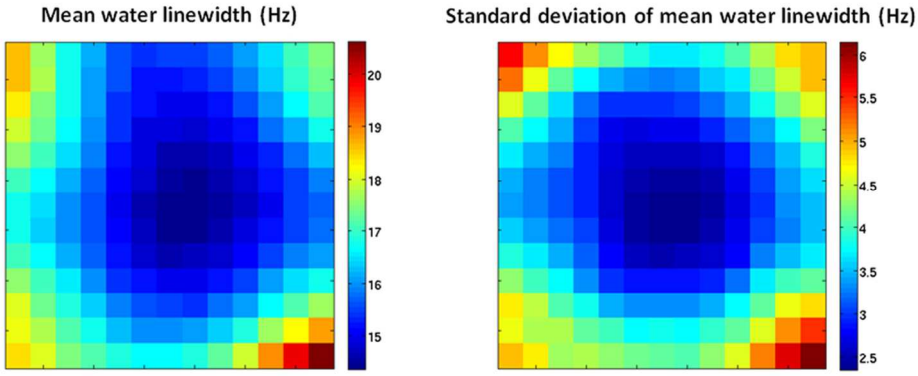


Figure 12. An illustrative overview of the setup of the study is provided in the upper panel. The concept of the automated planning software adopted in this study is illustrated in the lower left panel. The position and geometry of the VOI are illustrated in the lower right panel. The selection of the 13 x 13 matrix for quantification is indicated by the red dots. The voxel of which the spectra are displayed in figure 2 is shown in yellow.
102x43mm (300 x 300 DPI)

For Review Only

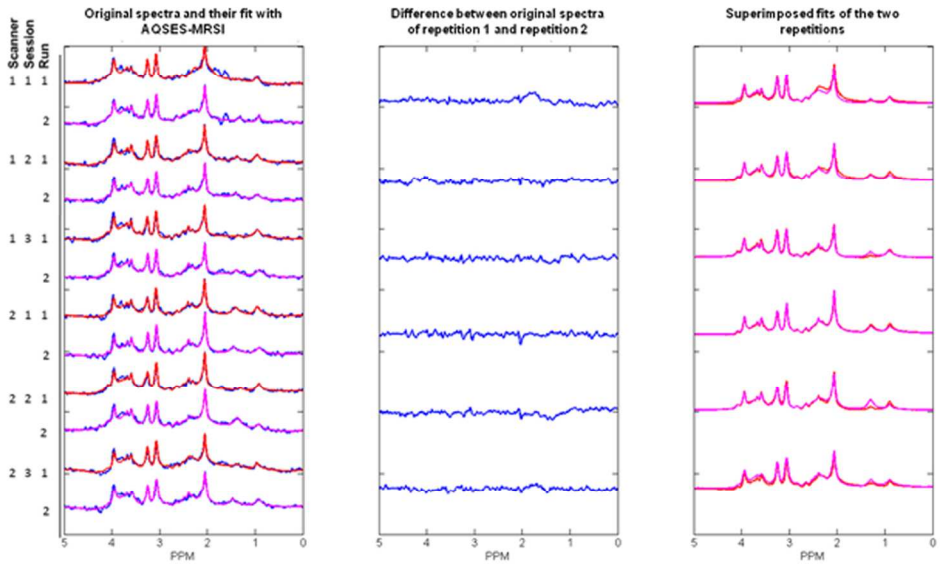


Figure 23. Comparison of spectra from the 12 examinations in one healthy volunteer, obtained from the voxel indicated in yellow in figure 1. Left: Original spectra and their fits with AQSES-MRSI. Center: Difference between original spectra of repetition 1 and repetition 2 at each time instance; some frequency misalignments are noticeable. Right: Superimposed fits of the two repetitions, including frequency shift corrections.
106x66mm (300 x 300 DPI)

VIEW ONLY

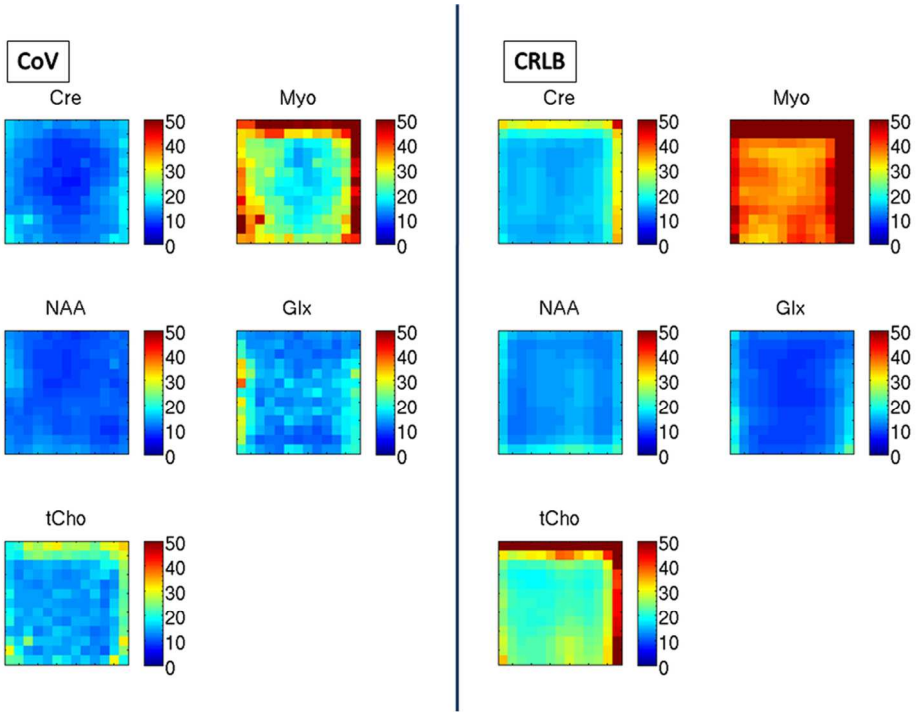


Figure 34. Maps of coefficient of variation (CoV) (left panel) and Cramér-Rao Lower Bounds (CRLB) (right panel) in the 13 x 13 matrix for NAA = N-acetyl aspartate; tCho = total choline; Cre = creatine; Glx = total of glutamine and glutamate; Myo = myo-inositol. Values are expressed in percentages.
121x85mm (300 x 300 DPI)

VIEW ONLY

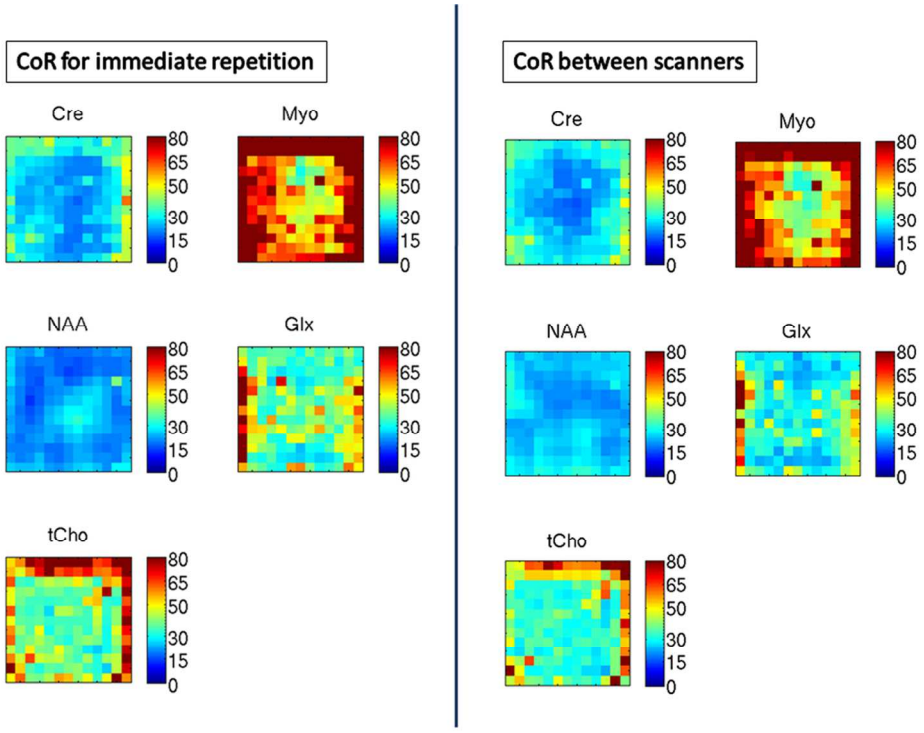


Figure 45. Maps of coefficient of repeatibility (CoR) for immediate repetition (left panel) and bewteen between scanners (right panel) in the 13 x 13 matrix for NAA = N-acetyl aspartate; tCho = total choline; Cre = creatine; Glx = total sum of glutamine and glutamate; Myo = myo-inositol. Values are expressed in percentages.
128x96mm (300 x 300 DPI)

EW ONLY

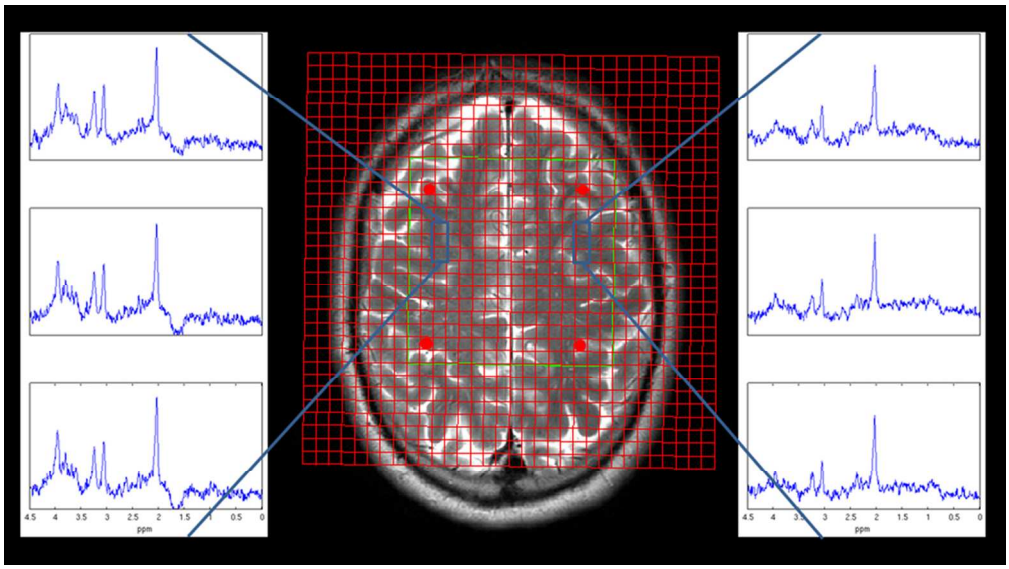


Figure 56. Illustration of the chemical shift displacement error of the slice selective refocusing pulses. Three voxels compared between the left and the right hemisphere, selected from the VOI overlaid on the T2-weighted anatomical image. Note the asymmetrical intensities of the spectra from the left hemisphere (affected by the chemical shift displacement artefact) compared to the spectra from the right hemisphere (not affected by the chemical shift displacement artefact). Some lipid contamination, most likely due to insufficient outer volume suppression of subcutaneous lipisds is visible in the spectra from the right hemisphere. The red dots indicate the selection of the 13 x 13 matrix, used for quantification.
95x53mm (300 x 300 DPI)

VIEW ONLY